Residual Structure in the Repeat Domain of Tau: Echoes of Microtubule Binding and Paired Helical Filament Formation†

David Eliezer,* Patrick Barré,‡ Muris Kobaslija,‡ Dylan Chan,‡ Xiaohua Li, and Lauren Heend

Department of Biochemistry and Program in Structural Biology, Weill Medical College of Cornell University, 1300 York Avenue, New York, New York 10021

Received May 23, 2004; Revised Manuscript Received November 5, 2004

ABSTRACT: The microtubule-associated protein tau is found aggregated into paired helical filaments in the intraneuronal neurofibrillary tangle deposits of victims of Alzheimer's disease (AD) and other related dementias. Tau contains a repeat domain consisting of three or four 31−32-residue imperfect repeats that forms the core of tau filaments and is capable of self-assembling into filaments *in vitro*. We have used high-resolution NMR spectroscopy to characterize the structural properties of the three-repeat domain of tau at the level of individual residues. We find that three distinct regions of the polypeptide corresponding to previously mapped microtubule interaction sites exhibit a preference for helical conformations, suggesting that these sites adopt a helical structure when bound to microtubules. In addition, we directly observe a marked preference for extended or β-strand-like conformations in a stretch of residues between two of the helical regions, which corresponds closely to a region previously implicated as an early site of β-strand structure formation and intermolecular interactions leading to paired helical filament (PHF) formation. This observation supports the idea that this region of the protein plays a crucial role in the formation of tau aggregates. We further show that disulfide-bond-mediated dimer formation does not affect and is not responsible for the observed structural preferences of the protein. Our results provide the first high-resolution view of the structural properties of the protein tau, are consistent with an important role for β structure in PHF formation, and may also help explain recent reports that tau filaments contain helical structure.

Protein aggregation is now believed to play a critical role in the pathogenesis and progression of a number of diseases, including important neurodegenerative syndromes such as Alzheimer's disease (AD)[1] and Parkinson's disease (for reviews, see refs *1*−*4*). The importance of protein aggregation in these diseases is supported by a number of observations, perhaps the most convincing of which is that genetic links to hereditary forms of these diseases have invariably been traced to genes that code either directly for the specific proteins that are found to be aggregated in each disease or for proteins responsible for modulating the production or destruction of the aggregating proteins (*5*).

The microtubule-associated protein tau, which can exist in six alternatively spliced forms in the central nervous system, is found in neurofibrillary tangles in AD in the form of hyperphosphorylated filamentous aggregates that appear as either straight filaments (SFs) or more typically as paired helical filaments (PHFs) (for reviews, see refs *6* and *7*). Currently, there are no known tau-associated mutations linked with AD, but several mutations in tau have recently been linked with a related neurodegenerative syndrome, frontotemporal dementia and Parkinsonism linked to chromosome 17 (FTDP-17) (*8*−*10*), supporting a causative role for tau aggregation in neuronal degeneration. This has led to greatly increased interest in the structural properties of tau PHFs and their mono- and oligomeric precursors and in the aggregation process that results in PHF formation. Unlike the case of amyloid fibrils found in extracellular AD plaques, even the general structural properties of PHFs remain controversial, with reports that they contain predominantly cross-β structure (a β-sheet-rich structure with β strands running perpendicular to the long axis of the fibrils) (*11*−*13*) at odds with reports reporting a lack of β-sheet structure (*14*), or even the presence of extensive α-helical structure (*15*, *16*). Nevertheless, it appears that a distinct region of tau is primarily responsible for the aggregation of the protein, namely, a region of imperfect 31−32-residue repeats, which is often considered the microtubule-binding domain of the protein but has also been shown to form the core of PHFs (*17*) and to assemble into PHF-like aggregates *in vitro* (*18*). In addition, recent studies of tau aggregation have implicated specific sequence motifs within the tau repeat region as being crucial for initiating the formation of PHFs (*19*, *20*).

Although it is found in an aggregated state in victims of AD, FTPD17, and other dementias, monomeric tau is a highly soluble protein. Nevertheless, despite great interest

† This work was supported in part by a New York City Council Speaker's Fund for Biomedical Research Award (to D.E.), the NIA, National Institutes of Health, Grant AG19391 (to D.E.), and a gift from Herbert and Ann Siegel (to D.E.).

* To whom correspondence should be addressed. E-mail: dae2005@med.cornell.edu. Telephone: 212-746-6557. Fax: 212-746-4843.

‡ These authors contributed equally to this work.

[1] Abbreviations: AD, Alzheimer's disease; SF, straight filament; PHF, paired helical filament; FTDP-17, frontotemporal dementia and Parkinsonism linked to chromosome 17; TFE, trifluoroethanol; ThT, thioflavin T; Aβ, β-amyloid peptide; APP, amyloid-β precursor protein.

10.1021/bi048953n CCC: $30.25
Published on Web 12/29/2004

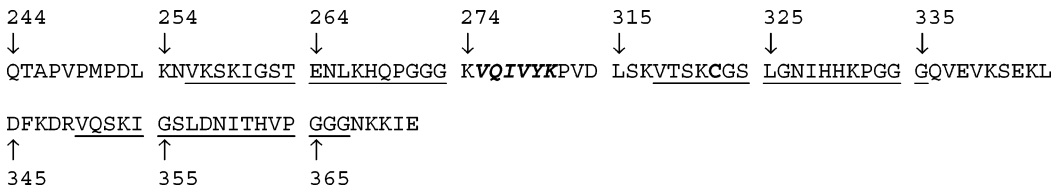

FIGURE 1: Sequence of tau fragment K19 corresponding to the microtubule-binding region of the three-repeat tau isoform. Residue numbering is based on the numbering of the longest tau isoform, htau40, and skips directly from residue 274 to 306 as a result of the absence of the second repeat (residues 275−305). The three 18-residue regions identified as microtubule-binding sites (*34*) are underlined. The 6-residue stretch implicated as a site of nascent β-sheet formation and PHF initiation (*19*) is in bold italic. Cys 322, which has been suggested to be crucial for PHF formation (*78*) is in bold.

in the structural properties of tau as they relate to both PHF formation and microtubule binding, no comprehensive high-resolution structural studies of tau have been reported, primarily because the protein is predominantly unfolded in solution (*14*, *21*) and therefore not amenable to techniques such as X-ray crystallography. Here, we report the results of high-resolution solution NMR structural studies of a fragment of tau comprising the microtubule-binding region of the three-repeat-containing isoforms of the protein. Our data show that the repeat region contains distinct segments with a preference for helical structure, which correspond to previously identified microtubule interaction sites. This observation suggests that these sites adopt helical structure when bound to microtubules. In addition, we show explicitly that a previously implicated PHF initiation site within the tau repeat region (*19*, *20*) exhibits an enhanced propensity for β-strand structure. Although disulfide-mediated dimer formation has been implicated to play an important role in tau self-assembly, we show that the structural preferences that we observe are not caused or affected by such dimer formation. Our results, which provide the first high-resolution view of the structural properties of tau, support the importance of local β structure in PHF formation while also offering a possible explanation for recent reports of helical structure in PHFs.

MATERIALS AND METHODS

Recombinant protein was expressed in *Escherichia coli* transfected with a PET vector construct containing the DNA sequence for a three-repeat microtubule-binding fragment of tau known as K19 under control of the strong T7 promoter (a kind gift from Dr. Peter Lansbury and Dr. Kenneth Kosik, Harvard Medical School). Similar to the naturally occurring three-repeat tau isoforms, K19 contains the first, third, and fourth microtubule-binding repeats of tau, consisting of residues 244−274 followed by residues 306−372 of the longest human tau isoform (Figure 1). A cysteine-free form of K19, C322A, was made by replacing Cys 322 with alanine using a Stratagene mutagenesis kit. Purification followed a protocol developed by our lab for studies of the Parkinson's disease protein α-synuclein (*22*). Briefly, cells were lysed by a freeze/thaw cycle followed by sonication and ultracentrifuged at 40 000 rpm in a Beckman ultracentrifuge using a Ti 50.2 rotor. The supernatant was subjected to a streptomycin sulfate precipitation, followed by two ammonium sulfate precipitations. The final pellet was resuspended in lysis buffer (1 mM EDTA, 1 mM DTT, 10 mM Tris, and 1 mM PMSF at pH 8.0), dialyzed against 25 mM Tris, 20 mM NaCl, 3 M urea, and 1 mM EDTA, applied to a cation-exchange column, and eluted using an NaCl gradient. Tau-containing fractions were pooled, dialyzed against 5% acetic acid, and purified on a C4 reverse-phase HPLC column using an acetonitrile gradient with 0.1% trifluoroacetic acid. Tau-containing fractions were lyophilized and stored at −20 °C and were highly pure as judged by SDS−PAGE, HPLC, and subsequent NMR spectroscopy.

NMR samples were prepared by dissolving lyophilized protein in sample buffer (100 mM NaCl and 10 mM Na_2HPO_4 at pH 7.4 in 90/10% H_2O/D_2O) and running the solution through a size-exclusion spin column or a 100-kDa filter to remove any protein aggregates. Protein concentrations were between 1 and 3 mg/mL. NMR spectra for performing resonance assignments were collected at 10 °C on a Varian INOVA 600 MHz NMR spectrometer equipped with four RF channels using modern versions of all experiments incorporating gradient coherence selection and sensitivity enhancement, in a manner similar to that used in previously reported studies (*22*, *23*). Typical collection parameters included spectral widths of 5400, 1600, 900, 9000, and 3400 Hz in the proton, nitrogen, CO, Cα/β, and Cα dimensions, respectively, with 1024 points in the direct dimension and 32 or 64 points in the indirect dimensions. Mixing times of 150 and 300 ms were used for NOESY−HSQC and HSQC−NOESY−HSQC data, respectively. $^3J_{HNH\alpha}$ coupling constants were measured using the HNHA experiment (*24*) with a homonuclear dephasing period of 25 ms. No correction was made for proton T1s because of the highly flexible nature of the tau K19 polypeptide. Data were processed with NMRPipe (*25*) using cosine or cosine-squared window functions and analyzed using NMRView (*26*). Spectra were referenced indirectly to DSS and ammonia (*27*) using the known chemical shift of water. Secondary shifts were calculated using recent random-coil values (*28*) as implemented in NMRView (*29*) with an additional correction for the pH dependence of histidine Cα and Cβ shifts (*30*). An attempt was made to correct for the sequence dependence of random-coil chemical shifts using two different recently reported sets of correction factors (*29*, *31*), but both of these led to considerably more scatter in the data and to larger deviations on average, indicating that the uncorrected values from ref *28* more closely approximate the true random-coil shifts under our conditions.

To monitor the kinetics of wild-type tau K19 dimer formation under oxidative conditions, samples were dissolved in buffer at different time points prior to loading onto a denaturing polyacrylamide gel under nonreducing conditions. The dimer band disappears under reducing conditions, confirming its identity. To assay for PHF formation, wild-type or C322A K19 samples were prepared exactly as for the NMR experiments described above and filament forma-

tion was triggered by the addition of 20 vol % trifluoroethanol (TFE). Protein concentrations prior to TFE addition were 1 mg/mL. Aggregation kinetics were monitored by recording the apparent UV absorption at 330 nm, which reports on changes in light scattering. Absorbance was measured in a Cary-50 spectrophotometer using a 1-cm pathlength, 1-mL volume quartz cuvette sealed to minimize evaporation. Reactions were found to be reasonably reproducible until about 10 h of data collection, after which large variations were observed between different runs, presumably because of evaporation and settling of large aggregates. After each reaction, the formation of filaments was assayed using thioflavin T (ThT) fluorescence and direct observation using electron microscopy. For the ThT assay, 40-μL aliquots of each sample were added to 960 μL of 20 mM Tris and 20 μM freshly filtered ThT at pH 8.0 and fluorescence spectra were collected using excitation at 450 nM. Control spectra were collected in the absence of protein and in the presence of unaggregated protein. In this assay, the presence of tau filaments is expected to result in greatly increased ThT fluorescence at ~480 nm. For electron microscopy, 10-μL aliquots of each sample were placed on a 400-mesh copper wire grid for 1 min, stained with 1.5% uranyl acetate for 1 min, and washed with doubly distilled water. Excess liquid was removed using filter paper, and samples were imaged using a JEOL 100CX-II scanning electron microscope using a magnification of 14000×. Circular dichroism spectra were collected on an AVIV 62 DS spectrometer equipped with a temperature controller from samples prepared exactly as above and using a 0.2-mm path-length cell.

RESULTS

The NMR proton−nitrogen correlation spectrum (HSQC) of the cysteine-free C322A mutant of the three-repeat tau fragment K19 (Figure 2a), collected under conditions where the protein is not aggregated into PHFs, shows poor resonance dispersion but relatively sharp lines, consistent with a largely unstructured polypeptide. Despite the high degree of resonance overlap, we were able to assign nearly all of the resonances from backbone nuclei in the C322A K19 fragment using triple-resonance experiments (Table 1S in the Supporting Information). An example stretch of connectivities (from residues Asp 306 to Leu 315) from both the HNCACB/CBCACONH and the HNCO/HNCACO pairs of experiments is shown in Figure 3. The data illustrate the poor resonance dispersion of the Cα resonances, with all three valines in this stretch having similar shifts in Figure 3a and the much better dispersion of the CO resonances in Figure 3b, which results from the sequence dependence of the CO shifts. In several instances, low-intensity satellite resonances were observed for residues adjacent to prolines, such as Gly271/Gly333/Gly365 and D252, presumably reflecting minor populations of cis-proline.

Figure 4a shows the deviation from the expected random-coil values of the Cα chemical shifts of C322A K19 as a function of the residue number. The Cα chemical-shift deviations (also known as secondary shifts) are known to be highly correlated with the ϕ and ψ backbone dihedral angles and therefore with secondary structure in proteins (*32*, *33*). Positive deviations correlate with a propensity toward helical structure, whereas negative deviations correlate with

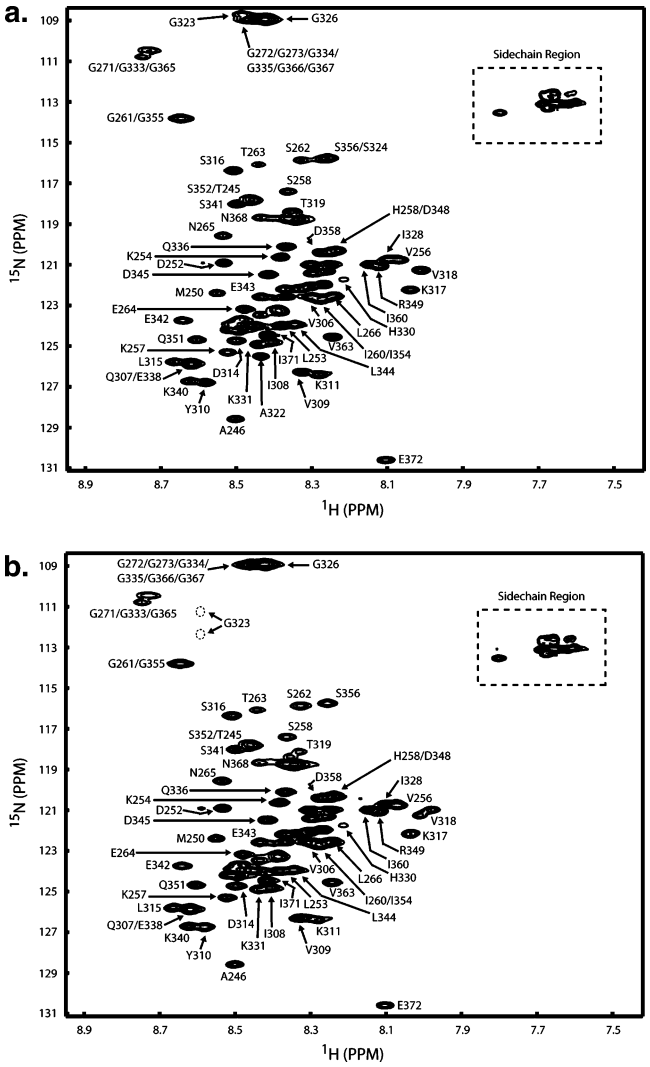

FIGURE 2: NMR proton−nitrogen correlation spectra of C322A (a) and wild-type (b) tau K19. Each resonance corresponds to an amide group in the protein. Resonances inside the hashed boxes correspond to side-chain amides. Sequence-specific assignments are indicated. The resonances for Gly 323 in the wild-type spectrum are below the contour level, and their locations are illustrated with dashed circles.

a propensity toward β structure. As can be seen in Figure 4a, most regions of the C322A K19 fragment of tau exhibit small positive deviations of the Cα chemical shifts, indicating a slight preference for helical conformations. Closer examination reveals that the positive deviations can largely be grouped into three distinct regions, consisting of residues 253−267, 315−328, and 346−361. The three regions are found approximately 31 residues apart, consistent with the length of the repeats in the microtubule-binding domain and correspond quite closely to the 18-residue regions originally identified as the sites responsible for the binding of tau to microtubules (*34*). Only a few regions of C322A K19 show negative deviations, with the most striking of these occurring between residues 307 and 312. This region contains five negative deviations of six total data points, of which two have magnitudes greater than 0.5 ppm. The consecutive nature of this stretch of negative chemical-shift deviations and the two data points of high magnitude indicate a higher propensity for extended β-strand-like conformations in this region than in the remainder of the protein. Two other regions

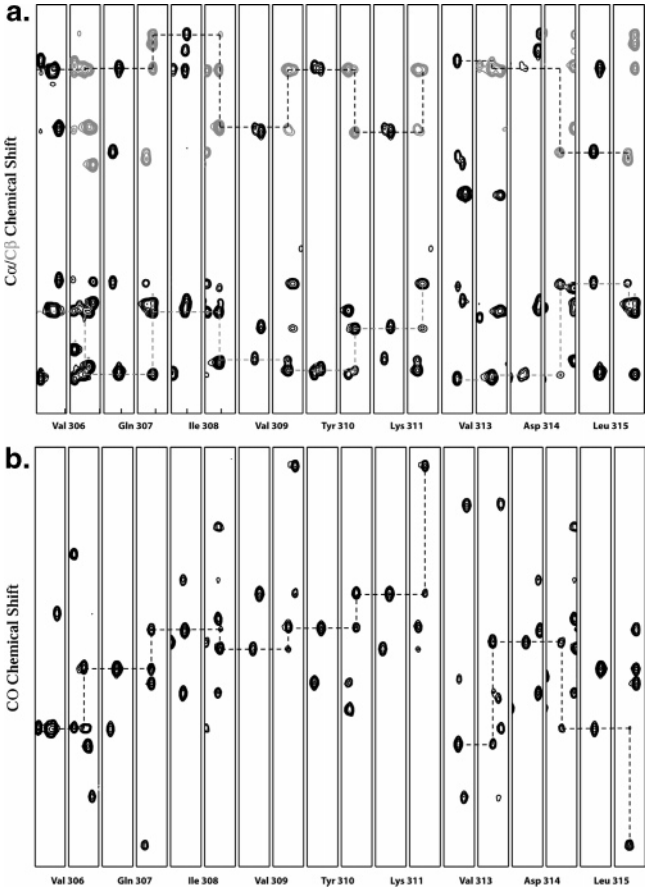

FIGURE 3: Data strips from triple-resonance HNCACB/CBCACONH (a) and HNCO/HNCACO (b) NMR experiments illustrating data quality, typical resonance dispersion, and sequential connectivities used to make resonance assignments.

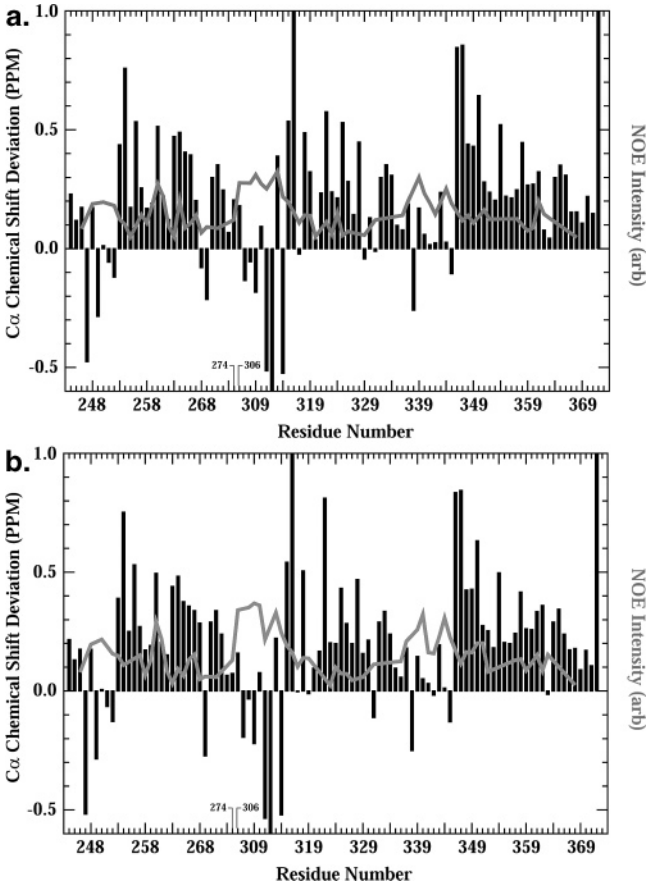

FIGURE 4: Deviations of the Cα chemical shifts of C322A (a) and wild-type (b) tau K19 from values expected for peptides in a random-coil ensemble of conformations. Positive deviations are associated with a propensity for helical conformations, while negative deviations are associated with extended strand-like structure. Overlaid on the Cα data are the corresponding HNHα(*i*, *i* − 1) NOE intensities.

of negative chemical-shift deviations, occurring between residues 247 and 252 and between residues 338 and 345, contain fewer and smaller magnitude deviations, making them less likely candidates for significant populations of *β* (or other secondary) structure.

To further evaluate the secondary structure propensities indicated by the Cα chemical shifts, we also examined the C*β* and CO chemical shifts, which we had obtained in the course of making sequence-specific resonance assignments. C*β* and CO shifts are also sensitive to backbone conformations, but they are typically less reliable than Cα shifts because CO shifts remain highly dispersed even in an unfolded structure and C*β* shifts are poorly dispersed even in a well-folded structure (*35*). Positive deviations of CO shifts and negative deviations of C*β* shifts are associated with helical structure. Figures 5a and 6a show the CO and C*β* secondary shifts for C322A K19 as a function of the residue number (note that the C*β* shifts are inverted for convenience), with the Cα secondary shifts from Figure 4a also shown for comparison. The data are considerably more scattered than the Cα data, as expected, and the trends described above are weaker. Nevertheless, the three distinct regions of positive Cα shifts contain nearly all of the observed positive CO and (inverted) C*β* deviations, despite also containing some negative deviations. In addition, the segments richest in negative Cα deviations exhibit consistently negative CO and (inverted) C*β* deviations. The segment from position 307 to 312 is dramatically conspicuous in the CO data and also clearly evident in the C*β* data as a highly contiguous stretch containing large-amplitude negative shift deviations.

In addition to chemical shifts, NMR coupling constants and NOEs can be used as experimental constraints on molecular conformations. Although these parameters are primarily useful in cases of well-formed protein structures, we measured vicinal HNHα coupling constants and short-range amide proton NOEs to look for further evidence of structure in tau K19. Because of the poor dispersion of two-dimensional NMR spectra of K19, we were only able to measure a restricted number (*34*) of HNHα coupling constants (not shown) using the HNHA experiment. Of these, all but three fell within the range of 6−7 Hz, which is consistent with a lack of well-formed secondary structure. Within this range of values, we did not observe any trends reflecting those evident in the chemical-shift data. This is likely a result of our inability to measure this parameter accurately enough to detect weak structural propensities. Similarly, we did not observe any sequential (or other) HN−HN NOE signals in HSQC−NOESY−HSQC data and only a handful of such signals in NOESY−HSQC spectra, where they were difficult to resolve and assign reliably. Although these NOEs can be observed in unstructured polypeptides under favorable circumstances (*36*), at the relatively low concentrations used here, they are not detectable in the absence of a well-formed helical structure (*37*). We were,

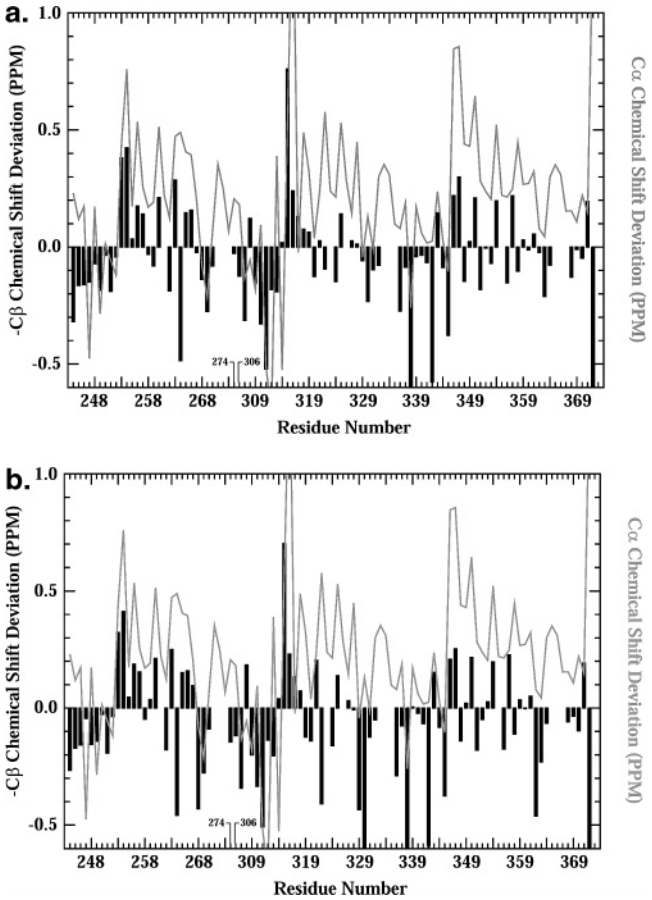

FIGURE 5: Deviations of the Cβ chemical shifts of C322A (a) and wild-type (b) tau K19 from values expected for peptides in a random-coil ensemble of conformations. Note the data are inverted for ease of comparison with the Cα data. Negative deviations (positive in the inverted data) are associated with a propensity for helical conformations, while positive deviations (negative in the inverted data) are associated with extended strand-like structure. Overlaid on the Cβ data are the corresponding Cα shift deviations.

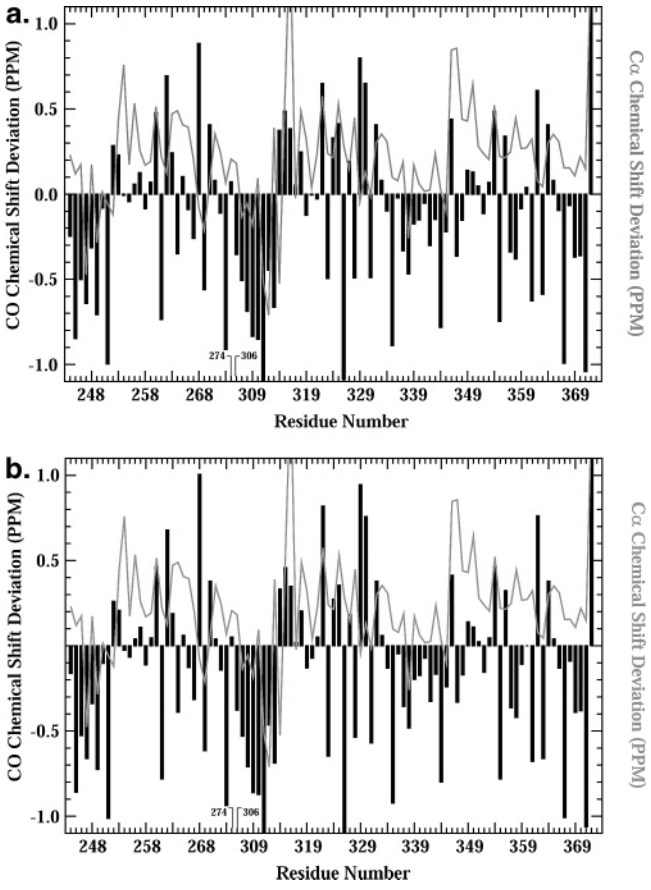

FIGURE 6: Deviations of the CO chemical shifts of C322A (a) and wild-type (b) tau K19 from values expected for peptides in a random-coil ensemble of conformations. Positive deviations are associated with a propensity for helical conformations, while negative deviations are associated with extended strand-like structure. Overlaid on the CO data are the corresponding Cα shift deviations.

however, able to observe and assign a large number of HNHα(i, i − 1) NOEs. These NOEs reflect a distance that is longer in helical structure and shorter in strand structure and should therefore be weak in helical regions and strong in strand regions. The intensity of the observed NOEs is overlayed onto the Cα secondary shift data in Figure 4a. It is clear that the regions of positive Cα shift deviations correspond nicely to regions of weak NOEs, whereas the regions of small or negative shift deviations contain the strongest NOE signals, with the region containing residues 307−312 showing the most intense NOE signals. Thus, the NOE data provide independent support for the secondary structure preferences inferred from the chemical-shift data.

Wild-type tau K19 contains a single Cys residue and is known to form disulfide-bond-linked dimers under oxidative conditions. To study the effect of disulfide bond cross-linking of K19 monomers on the structural properties of the protein, we collected an equivalent set of NMR data for wild-type K19 prepared as described above (i.e., under oxidative conditions) and assigned the backbone resonances independently of the C322A assignments (Table 2S in the Supporting Information). SDS−PAGE under nonreducing conditions demonstrated that samples prepared in this manner contained a large fraction of covalently linked K19 dimers. Dimerization takes place on a time scale of several hours

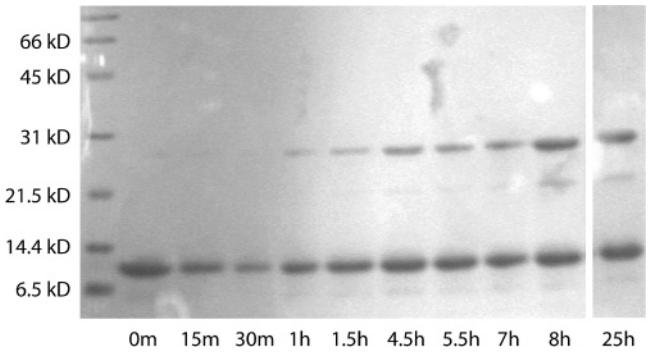

FIGURE 7: Time course of wild-type tau K19 dimer formation monitored by nonreducing SDS−PAGE. Protein samples were dissolved at different times prior to loading onto the gel, as indicated. Lanes between 8 and 25 h were excised.

but does not appear to proceed to completion, with about half of the protein remaining monomeric after 24 h (Figure 7) and even after several weeks in the NMR tube (Figure 1S in the Supporting Information and data not shown). To minimize the effects of dimer formation during NMR data collection, wild-type K19 samples were typically prepared a day ahead of time. Although a small degree of dimerization probably continues to occur on the time scale of the NMR experiments used for chemical-shift assignments (several days for each experiment), any effects on the data must be insignificant, because successive triple-resonance spectra do

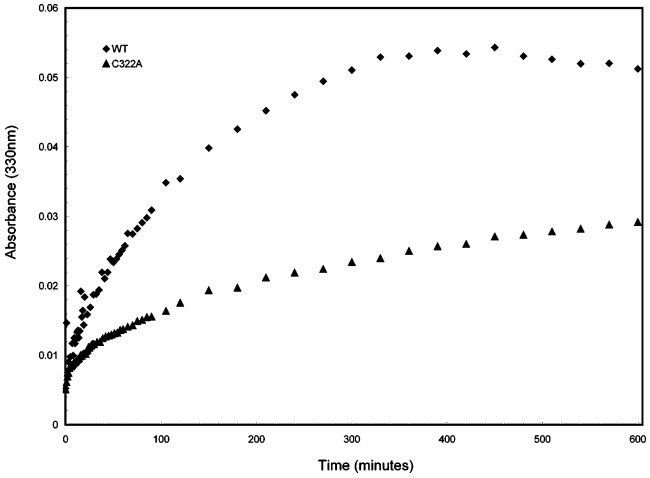

FIGURE 8: Kinetic traces of TFE-induced C322A and wild-type K19 aggregation as monitored by light scattering, reflected as UV absorbance at 330 nm.

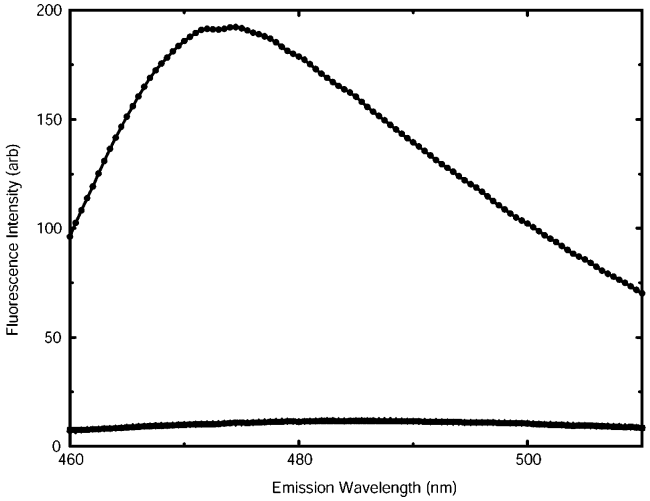

FIGURE 9: ThT fluorescence after excitation at 450 nm in the presence of K19 aggregates induced by the addition of TFE. PHF-like filaments are expected to lead to a specific and dramatic increase in ThT fluorescence intensity at 480 nm, as observed. Control spectra using no protein or unaggregated protein are overlapped at the bottom of the plot and show little fluorescence at 480 nm.

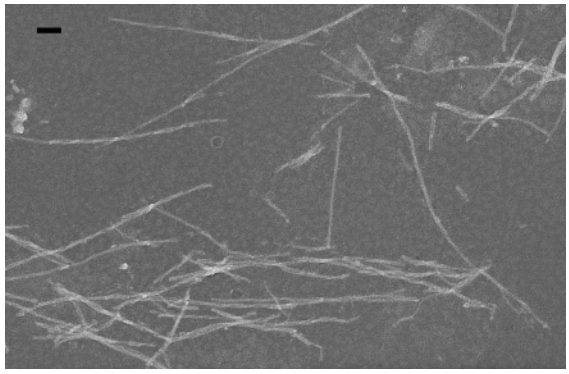

FIGURE 10: Electron micrographs of tau K19 filamentous aggregates induced by the addition of TFE. The horizontal black bar represents a length scale of 100 nm.

not show any perturbations in resonance positions or spectral quality. Proton−nitrogen correlation spectra from dimer-containing wild-type K19 samples (Figure 2b) were highly similar to those of C322A K19, except that several resonances (for example, Val 318, Thr 319, and Gly 323) originating from residues near position 322 were observed to be doubled as well as weaker in intensity and no resonance was detectable for Cys 322 itself. Resonances from Cys 322 were, however, detectable as $i - 1$ correlations in several three-dimensional experiments. Interestingly, these resonances could be attributed to the reduced form in the CBCACONH spectrum and to the oxidized form in the NOESY−HSQC spectrum based on the unique chemical shifts of the two forms. The doubled resonances near Cys 322 almost certainly reflect the simultaneous presence of mono- and dimeric protein populations and indicate that both give rise to detectable NMR signals. Their weak intensities and the absence of the Cys resonance(s) may reflect the lower effective concentration of each species and possibly a slow conformational exchange process near the cysteine or cystine site. Cα chemical-shift deviations from both resonances of each doubled peak were identical, indicating no difference in local secondary structure between the mono- and dimeric forms.

A comparison of the Cα, Cβ, and CO chemical-shift deviations and the HNHα NOE intensities of wild-type K19 (Figures 4b, 5b, and 6b) with those of C322A reveals only minor differences. These observations demonstrate that neither disulfide bond formation nor the C322A mutation significantly alters the structural preferences of the tau K19 polypeptide. The very close agreement of the chemical-shift deviations determined completely independently for the wild-type and the C322A mutant constructs is also useful as an indicator of the reproducibility and significance of these measurements.

To confirm the ability of our recombinant tau fragment K19 and of the C322A mutant K19 fragment to form PHF-like aggregates *in vitro*, we used a combination of light scattering, ThT fluorescence, and electron microscopy. Incubation of both K19 and C322A K19 in the presence of 20% TFE resulted in a progressive increase in light scattering at 330 nm (Figure 8), indicating the formation of oligomeric colloidal particles. The choice of TFE to induce filament formation was motivated by its common use in studies of amyloid fibril formation (for example, see ref *38*) and by the fact that TFE-induced tau PHF formation has not been previously reported, although hexafluoroisopropanol, which often effects polypeptides in a manner similar to TFE, has been shown to induce PHF assembly (*39*) and TFE is known to enhance heparin-induced tau self-assembly (*40*). Circular dichroism data indicate that the reproducible initial phase of oligomerization results in an increase in helical structure (not shown), whereas only further incubation, showing irreproducible kinetics with a time constant of hours to days, leads to β structure. After such further incubation, the presence of tau filaments was confirmed by a large increase in the fluorescence of ThT when excited at 450 nm (Figure 9), and the direct observation of filamentous aggregates in negatively stained electron micrographs (Figure 10) that resemble typical PHFs, with the characteristic twisted filament appearance, widths of approximately 20 nm, and cross-over spacings of approximately 100 nm. Interestingly, under these conditions, we did not observe any clear increase in the rate of oligomer formation for the disulfide-bond-forming wild-type protein (Figure 8) as measured by the time required to reach the midpoint of each reaction (ap-

proximately 120 min). This may be a result of using TFE, which appears to be an extremely potent inducer of aggregation and may mask variations observed under different conditions. The difference in the signal amplitude achieved in the wild-type and mutant K19 reactions may be due either to a difference in the total amount of tau aggregates or to differences in the average size of the aggregates produced (*41*). A more detailed understanding of the TFE-induced assembly process will require further investigation.

DISCUSSION

Amyloid Fibrils Versus PHFs. Protein aggregation appears to be intimately related to a large and growing number of diseases, including a number of brain disorders such as AD and Parkinson's disease (*1*−*4*). Almost all of these disorders feature aggregates that fall into the category of amyloid fibrils, and this has led to an intense interest in the process of amyloid fibril formation. A large number of studies have reported results related to the structure of the fibrils themselves, the unaggregated precursor proteins, and oligomeric species along the fibril-formation pathway, and some information is also available regarding the fibril-formation process, which necessarily involves transitions among these different species (*42*).

In the case of AD, two different proteins form aggregates that are found in two different proteinaceous deposits: the β-amyloid peptide (Aβ) is found in the extracellular amyloid plaques, and the microtubule-associated protein tau is found in the intracellular neurofibrillary tangles (for review, see ref *43*). Aβ is a short 40- or 42-residue peptide that is formed by the proteolytic processing of the amyloid precursor protein (APP). Mutations linked to hereditary cases of AD have been identified both in the gene coding for APP, including some mutations within the Aβ sequence itself, and in the gene encoding for the γ-secretase protease responsible for generating Aβ from APP (for review, see ref *44*). The aggregated state of Aβ found in amyloid plaques has been extensively characterized and constitutes the prototypical amyloid fibril, possessing a characteristic cross-β structure rich in β-sheet secondary structure, which is oriented in a direction perpendicular to the long fibril axis and twists around this axis in a super-helical fashion (*11*, *45*). Recent studies have elucidated many of the detailed molecular and intermolecular interactions of the Aβ peptide that underpin the morphological features of Aβ amyloid fibrils (*46*−*48*).

Tau PHFs appear to be somewhat unusual in that they do not obviously fall into the category of amyloid fibrils. PHFs are generally reported to be thicker than amyloid fibrils (∼20 nm in width versus ∼10 nm in width for amyloid fibrils), although the dimensions of both types of fibrils appear to be rather variable. In addition, amyloid fibrils are invariably highly enriched in β-sheet structure, whereas considerable controversy remains regarding the secondary structure content of PHFs (*11*−*16*). Nevertheless, the appearance of PHFs in a large number of neurodegenerative disorders, combined with the recent genetic linkage of tau to a specific subclass of these disorders (*8*−*10*), suggests that PHF formation, much like amyloid fibril formation, may play an important role in the pathogenesis of neuronal degeneration. Understanding the details of PHF formation may therefore help to clarify the role of tau and its aggregated forms in disease.

Structural Echoes of Microtubule Binding. To gain insight into the structural features of tau and how they may relate to both its normal microtubule-binding function and its disease-related PHF-forming ability, we investigated the properties of the microtubule-binding and PHF core-forming region of the protein, tau K19, at high-resolution using NMR spectroscopy. Previous studies of tau in solution have used primarily optical methods such as circular dichroism and Fourier transform infrared spectroscopy to show that the protein exists in a predominantly unfolded conformational ensemble (*14*, *21*). The poor dispersion of the NMR proton−nitrogen correlation spectrum of tau K19 supports this conclusion (Figure 2), because a lack of resonance dispersion reflects a lack of heterogeneity in the local environments of individual residues in a protein sequence. However, the deviations of NMR carbon chemical shifts from their random-coil values combined with short-range NOEs (Figures 4−6) provide a much more detailed look at the structural properties of tau K19 by revealing the conformational preferences of the protein at each individual residue's location throughout the sequence.

In well-folded globular proteins, Cα chemical-shift deviations typically have magnitudes of 2−3 ppm (*49*). In contrast, our data for tau K19 show deviations that are generally less than 0.5 ppm. This confirms that tau K19 is indeed primarily unfolded and that this is true throughout its sequence. Nevertheless, even unfolded proteins are often found to possess residual secondary structure, which frequently bears a relationship to structure that is formed in the properly folded state. Examples of this include typical globular proteins or domains such as staphylococcal nuclease (*50*), myoglobin (*51*, *52*), and the IgG-binding domain of protein L (*53*), as well as intrinsically unstructured proteins such as $p27^{Kip1}$ (*54*), the transactivation domains of CREB (*55*) and c-Myb (*56*), and α-synuclein (*22*, *37*), which adopt a well-defined structure only upon binding to their partners. Evidence of residual helical structure is visible in three regions of tau K19, comprising residues 253−267, 315−328, and 346−361, which exhibit consistently positive Cα chemical-shift deviations, the majority of the positive CO and inverted Cβ chemical-shift deviations, and weak HNα NOEs. Interestingly, these regions also correspond quite closely to the 18-residue regions, spanning residues 256−273, 318−335, and 350−367, which have been implicated as microtubule-binding sites (*34*) [note that other regions of tau outside the repeat region are also implicated in microtubule binding (*57*)]. Although the three residual structure regions are slightly shorter (15, 14, and 16 residues, respectively), this might be expected because the final four residues of each microtubule interaction site form a PGGG motif that is highly unlikely to adopt helical structure and has been proposed to bind to a β-tubulin pocket on the inside of microtubules in an extended conformation (*58*).

Because residual structure typically reflects the native-state structure, because the only context in which tau is believed to adopt a well-formed structure is upon binding to microtubules, and because the residual helical character that we observe closely overlaps the non-PGGG portion of the previously identified microtubule-binding sites, it is likely that these regions adopt a stable helical structure when in the microtubule-bound state of tau. To our knowledge this is the first glimpse, albeit an indirect one, into the structural

properties of tau in the microtubule-associated state. Although several NMR studies of short peptides corresponding to individual tau repeats have been reported (*59*, *60*), these studies were performed in the presence of organic solvents known to be potent inducers of helical structure, making it difficult to interpret their relevance to the properties of the protein under physiological conditions. Interestingly, a recent NMR study of specific Ser-Pro and Thr-Pro phosphorylation motifs in full-length tau (*61*), none of which are present within the repeat domain of the protein, suggests that the remainder of the protein possesses little or no residual structure, supporting the hypothesis, based on our data, that the repeat domain is critical to the formation of structure in the context of both microtubule interactions and filament formation.

Residual β-Strand Structure and Filament Formation. Another noteworthy feature in the tau K19 Cα data is the presence of a 6-residue region of mostly negative chemical-shift deviations from residue 307 to 312. This region is particularly interesting because of recent results that have implicated the six residues from Val 306 to Lys 311 (termed PHF6) as a potential nucleation site for the formation of tau PHFs (*19*, *20*). Furthermore, formation of β structure within PHF6 was suggested to be critical for the ability of this site to nucleate PHFs, and it was suggested that FTPD17-linked mutations promote PHF formation by enhancing β structure at PHF6 or at a similar site, PHF6*, in four-repeat tau isoforms (*20*). Our data, consisting of a combination of Cα, Cβ, and CO shifts, as well as HNHα NOEs, directly confirm that PHF6 is in fact the region of strongest β-structure propensity within the three-repeat region of tau and are consistent with the possibility that this region may play a key role in the early steps leading to PHF formation.

Models for PHF Core Structure. The structural properties of PHFs remain a subject of considerable controversy, with even recent reports providing conflicting pictures of β-sheet versus α-helix structure content. X-ray and electron diffraction studies show clear evidence for cross-β structure in PHFs (*13*), while circular dichroism data indicate an entirely α-helical (*15*) or a mixed α/β structure (*16*). Our observation of a propensity for β structure in exactly the region implicated to nucleate PHF formation in previous work (*19*, *20*) suggests that the formation of nascent β structure may in fact be a critical step in PHF formation. In this case, it seems probable that such elements of early β structure would persist in the mature PHF [although there is precedent in studies of the folding of globular proteins for the formation of transient, non-native, secondary structure that is not found in the final folded structure (*62*, *63*)]. Even small regions of β structure, if properly packed in the PHF core, could potentially account for the 4.7 Å spacing observed in PHF diffraction patterns (*13*). On the other hand, our data also clearly show that much of the tau K19 microtubule-binding domain has a preference for helical conformations. The close overlap between regions of helical propensity and microtubule affinity suggests that this structural preference reflects the microtubule-bound structure of the protein. However, other compact conformations or close intermolecular contacts, such as would be expected to occur during oligomerization leading to PHF formation, may suffice to drive these regions of the protein into helical conformations. This helical structure could potentially explain the circular-dichroism-based observations of helical structure in PHFs as well as our own observations of helical oligomeric structures during the early stages of TFE-induced aggregation.

One model based on our results that could explain the conflicting data on the secondary structure content of PHFs is that relatively short segments of tau form β structure that is packed in a cross-β conformation at the PHF core and is crucial for early steps in PHF assembly, while other segments of tau form helical structure that may or may not be crucial for PHF integrity. Such helical structure could occur in the microtubule-binding regions of the PHF core-forming repeat domain, in which case it would be involved in interactions that are sufficiently stable to protect it from proteolytic cleavage (*17*) and could also play a role in stabilizing the PHF structure. Alternately, such structure could occur in the N- or C-terminal domains of tau, where it would be susceptible to removal by proteolytic cleavage (*17*) and would be unlikely to play any significant role in PHF stability or formation. In either case, the observation of predominantly helical structure in circular dichroism spectra of PHFs (*15*) could be explained by a relatively small fraction of the protein adopting β-sheet structure (as little as one or two stretches of six residues), while a much larger fraction of the protein (the largest tau isoform contains 441 residues) adopts α-helical structure. A similar model proposing only short stretches of β-strand structure in tau PHFs has been described in an effort to explain the lack of evidence for significant amounts of β structure in studies of tau PHFs (*19*), but this model did not include any insights into structure outside the small β-sheet-rich core and how such structure may account for evidence of helical structure in tau PHFs. The plausibility of such a model is supported by the fact that many small peptides are known to form typical cross-β-structure-containing amyloid fibrils (for example, see refs *64*−*66*) and by several models of amyloid fibrils, which envision a small core containing cross-β structure decorated by domains of peripheral structure that are not involved in fibril-stabilizing interactions (*67*−*69*).

Predicted Effects of Disease-Linked Mutations. Our observations of residual secondary structure elements in tau K19 make it interesting to consider the potential effects on such structure of disease-linked tau mutations and whether such effects may be related to the previously characterized influence of these mutations on tau function and self-assembly. FTDP-17-linked point mutations within K19 include K257T, G272V, V337M, and K369I. Each of these mutations has been reported to perturb tau-promoted microtubule assembly and to increase the rate of tau self-assembly (*41*, *70*−*75*). On the basis of the conformational preferences of individual amino acids as tabulated by Chou and Fasman (*76*), the effects of each of these mutations on the residual structure of the protein can be anticipated. K257T replaces a helix-favoring lysine with a β-strand-preferring threonine and does so in the middle of the first of the three identified regions of helical-structure propensity (residues 253−272). Thus, this mutant may be expected to disrupt this region of residual structure. This expectation is supported by the helix-propensity-predicting algorithm AGADIR (*77*), which correctly identifies the first (but not the second and third) of the three regions of residual helical structure that we observe and predicts that the K257T mutant would significantly reduce helix propensity in this region. If, as we hypothesize,

this region interacts with microtubules in a helical conformation, this structural perturbation could interfere with the microtubule interactions of this site. In addition, if β-strand structure is propagated throughout the tau repeat region in PHFs, this mutation would be expected to favor a local transition to such structure, possibly accelerating PHF formation. Evaluation of this hypothesis will require further structural studies using this mutant.

The other three FTPD-linked mutations under consideration fall outside the identified regions of residual helical structure, precluding an analysis of their effects using AGADIR. In addition, because we do not have a model for the structure adopted at the sites of these mutations upon microtubule binding, we cannot assess how they may perturb such binding. However, two of the mutations, G272V and K369I, replace residues that are a very poor choice for β secondary structure with ones that are excellent β-strand formers. G272V nearly abuts the region of the protein that we observe to be most prone toward β structure and could enhance the β-strand propensity of this area and thereby promote self-assembly. A greater propensity for β-strand structure at position 369 could also favor filament formation if the β conformation propagates to the end of the fourth repeat, but as discussed above, this remains uncertain. In contrast to the other three mutations, the mutation V337M does not favor β structure. Instead, it replaces a β-strand-preferring valine with a helix-preferring methionine. It is possible that the increase in hydrophobicity at this site plays a role in promoting aggregation, but any structural basis for how this mutation perturbs microtubule binding or enhances PHF formation remains unclear at present.

The above analysis of disease-linked tau mutations, particularly K257T and G272V, supports our hypothesis that the residual structure that we observe is relevant to both the microtubule-binding and self-assembly interactions of the tau repeat region. Further studies will be required, however, to firmly establish this hypothesis, including direct confirmation of the expected effects of the mutations on the structural properties of the protein and more careful analysis of the effects of the mutations on both microtubule interactions and self-assembly. The former is necessary to address the somewhat ambiguous previous results regarding the effects of the mutations on microtubule affinity, as opposed to microtubule assembly (*73*), and to more carefully quantify the influence of the mutations on the specific construct being used, because different results have been reported for different tau constructs (*72*).

Role of Disulfide-Bond-Mediated Dimer Formation. An additional complication regarding the formation of PHFs from tau monomers is the potential involvement of intermolecular disulfide bond formation (*78*). To address this issue, we compared the structural properties of wild-type and C322A tau K19. Our results indicate that the presence or absence of the cysteine does not affect the structural characteristics that we were able to observe, including the three regions of residual helical structure and the preference for β-strand structure at the PHF6 site. In addition, dimerization of the wild-type protein does not affect these structural features either. On the basis of these observations, we conclude that the previously reported effects of disulfide-bond-mediated tau K19 dimerization on self-assembly rates do not originate directly from structural changes of the protein induced by dimerization. Such effects are more likely to originate from an effective increase in local protein concentration, as previously suggested (*19*), leading to an enhanced rate of intermolecular interactions. We also observed that both tau K19 constructs formed morphologically similar PHF-like aggregates with similar rates of initial oligomerization upon incubation in the presence of TFE. We therefore conclude, in agreement with recent results (*79*, *80*), that disulfide bond formation, while potentially accelerating PHF formation, is not a prerequisite for it. We note that disulfide bond formation was proposed to be a crucial step in early studies of amyloid fibril formation by the protein transthyretin (*81*) but was later shown not to be required (*82*).

CONCLUSIONS

Our results, based upon high-resolution NMR studies of the K19 three-repeat microtubule-binding domain of tau, suggest that the microtubule-binding sites within the repeat domain may adopt helical structure in the microtubule-bound state of tau. Our results also support a model of PHF formation in which regions of nascent β structure play an important initiation role. These conclusions are consistent with the expected effects of disease-linked tau mutations on the observed residual structure of tau K19. We also provide a possible explanation for disparate claims regarding the α- or β-structure content of PHFs, by proposing that the cross-β structure at the core of PHFs may be limited to relatively short stretches of the protein, while other regions of the protein, either within the repeat region or in the C- or N-terminal domains, adopt helical conformations, leading to the observed high content of α-helical structure. Finally, our results indicate that disulfide-bond-mediated dimerization of tau K19 does not directly alter the structural properties of the protein.

ACKNOWLEDGMENT

We thank Dr. Peter Lansbury and Dr. Kenneth Kosik (Harvard Medical School) for valuable discussions and for generously providing us with the K19 gene construct and Gillian Browne, Trudy Ramlall, and Carla Rospigliosi for technical assistance.

SUPPORTING INFORMATION AVAILABLE

Figure comparing and showing the dimerization state of an NMR sample of wild-type tau K19 after 9 days and resonance assignment tables for the wild-type and C322A proteins. This material is available free of charge via the Internet at http://pubs.acs.org.

REFERENCES

1. Walker, L. C., and LeVine, H. (2000) The cerebral proteopathies: Neurodegenerative disorders of protein conformation and assembly, *Mol. Neurobiol. 21*, 83−95.
2. Koo, E. H., Lansbury, P. T., Jr., and Kelly, J. W. (1999) Amyloid diseases: Abnormal protein aggregation in neurodegeneration, *Proc. Natl. Acad. Sci. U.S.A. 96*, 9989−9990.
3. Dobson, C. M. (2001) Protein folding and its links with human disease, *Biochem. Soc. Symp*, 1−26.
4. Trojanowski, J. Q., and Lee, V. M. (2002) Parkinson's disease and related synucleinopathies are a new class of nervous system amyloidoses, *Neurotoxicology 23*, 457−460.

5. Lansbury, P. T., Jr. (1999) Evolution of amyloid: What normal protein folding may tell us about fibrillogenesis and disease, *Proc. Natl. Acad. Sci. U.S.A. 96*, 3342−3344.
6. Mandelkow, E. M., and Mandelkow, E. (1998) Tau in Alzheimer's disease, *Trends Cell Biol. 8*, 425−427.
7. Goedert, M., and Spillantini, M. G. (2000) Tau mutations in frontotemporal dementia FTDP-17 and their relevance for Alzheimer's disease, *Biochim. Biophys. Acta 1502*, 110−121.
8. Hutton, M., Lendon, C. L., Rizzu, P., Baker, M., Froelich, S., Houlden, H., Pickering-Brown, S., Chakraverty, S., Isaacs, A., Grover, A., Hackett, J., Adamson, J., Lincoln, S., Dickson, D., Davies, P., Petersen, R. C., Stevens, M., de Graaff, E., Wauters, E., van Baren, J., Hillebrand, M., Joosse, M., Kwon, J. M., Nowotny, P., and Heutink, P. et al. (1998) Association of missense and 5′-splice-site mutations in tau with the inherited dementia FTDP-17, *Nature 393*, 702−705.
9. Spillantini, M. G., Murrell, J. R., Goedert, M., Farlow, M. R., Klug, A., and Ghetti, B. (1998) Mutation in the tau gene in familial multiple system tauopathy with presenile dementia, *Proc. Natl. Acad. Sci. U.S.A. 95*, 7737−7741.
10. Poorkaj, P., Bird, T. D., Wijsman, E., Nemens, E., Garruto, R. M., Anderson, L., Andreadis, A., Wiederholt, W. C., Raskind, M., and Schellenberg, G. D. (1998) Tau is a candidate gene for chromosome 17 frontotemporal dementia, *Ann. Neurol. 43*, 815−825.
11. Kirschner, D. A., Abraham, C., and Selkoe, D. J. (1986) X-ray diffraction from intraneuronal paired helical filaments and extraneuronal amyloid fibers in Alzheimer disease indicates cross-β conformation [published erratum appears in *Proc. Natl. Acad. Sci. U.S.A.* 1986 Apr, *83*, 2776], *Proc. Natl. Acad. Sci. U.S.A. 83*, 503−507.
12. Giannetti, A. M., Lindwall, G., Chau, M. F., Radeke, M. J., Feinstein, S. C., and Kohlstaedt, L. A. (2000) Fibers of tau fragments, but not full length tau, exhibit a cross β-structure: Implications for the formation of paired helical filaments, *Protein Sci. 9*, 2427−2435.
13. Berriman, J., Serpell, L. C., Oberg, K. A., Fink, A. L., Goedert, M., and Crowther, R. A. (2003) Tau filaments from human brain and from *in vitro* assembly of recombinant protein show cross-{β} structure, *Proc. Natl. Acad. Sci. U.S.A. 100*, 9034−9038.
14. Schweers, O., Schonbrunn-Hanebeck, E., Marx, A., and Mandelkow, E. (1994) Structural studies of tau protein and Alzheimer paired helical filaments show no evidence for β-structure, *J. Biol. Chem. 269*, 24290−24297.
15. Sadqi, M., Hernandez, F., Pan, U., Perez, M., Schaeberle, M. D., Avila, J., and Munoz, V. (2002) α-Helix structure in Alzheimer's disease aggregates of tau-protein, *Biochemistry 41*, 7150−7155.
16. Goux, W. J. (2002) The conformations of filamentous and soluble tau associated with Alzheimer paired helical filaments, *Biochemistry 41*, 13798−13806.
17. Wischik, C. M., Novak, M., Edwards, P. C., Klug, A., Tichelaar, W., and Crowther, R. A. (1988) Structural characterization of the core of the paired helical filament of Alzheimer disease, *Proc. Natl. Acad. Sci. U.S.A. 85*, 4884−4888.
18. Crowther, R. A., Olesen, O. F., Jakes, R., and Goedert, M. (1992) The microtubule binding repeats of tau protein assemble into filaments like those found in Alzheimer's disease, *FEBS Lett. 309*, 199−202.
19. von Bergen, M., Friedhoff, P., Biernat, J., Heberle, J., Mandelkow, E. M., and Mandelkow, E. (2000) Assembly of tau protein into Alzheimer paired helical filaments depends on a local sequence motif ((306)VQIVYK(311)) forming β structure, *Proc. Natl. Acad. Sci. U.S.A. 97*, 5129−5134.
20. von Bergen, M., Barghorn, S., Li, L., Marx, A., Biernat, J., Mandelkow, E. M., and Mandelkow, E. (2001) Mutations of tau protein in frontotemporal dementia promote aggregation of paired helical filaments by enhancing local β-structure, *J. Biol. Chem. 276*, 48165−48174.
21. Cleveland, D. W., Hwo, S. Y., and Kirschner, M. W. (1977) Physical and chemical properties of purified tau factor and the role of tau in microtubule assembly, *J. Mol. Biol. 116*, 227−247.
22. Eliezer, D., Kutluay, E., Bussell, R., Jr., and Browne, G. (2001) Conformational properties of α-synuclein in its free and lipid-associated states, *J. Mol. Biol. 307*, 1061−1073.
23. Bussell, R., Jr., and Eliezer, D. (2001) Residual structure and dynamics in Parkinson's disease-associated mutants of α-synuclein, *J. Biol. Chem. 276*, 45996−46003.
24. Vuister, G. W., and Bax, A. (1993) Quantitative J correlation: A new approach for measuring homonuclear three-bond J(HNHα) coupling constants in ^{15}N-enriched proteins, *J. Am. Chem. Soc. 115*, 7772−7777.
25. Delaglio, F., Grzesiek, S., Vuister, G. W., Zhu, G., Pfeifer, J., and Bax, A. (1995) NMRPipe: A multidimensional spectral processing system based on UNIX pipes, *J. Biomol. NMR 6*, 277−293.
26. Johnson, B. A., and Blevins, R. A. (1994) NMRView: A computer program for the visualization and analysis of NMR data, *J. Biomol. NMR 4*, 603−614.
27. Wishart, D. S., Bigam, C. G., Yao, J., Abildgaard, F., Dyson, H. J., Oldfield, E., Markley, J. L., and Sykes, B. D. (1995) ^{1}H, ^{13}C, and ^{15}N chemical shift referencing in biomolecular NMR, *J. Biomol. NMR 6*, 135−140.
28. Wishart, D. S., Bigam, C. G., Holm, A., Hodges, R. S., and Sykes, B. D. (1995) ^{1}H, ^{13}C, and ^{15}N random coil NMR chemical shifts of the common amino acids. I. Investigations of nearest-neighbor effects, *J. Biomol. NMR 5*, 67−81.
29. Schwarzinger, S., Kroon, G. J., Foss, T. R., Chung, J., Wright, P. E., and Dyson, H. J. (2001) Sequence-dependent correction of random coil NMR chemical shifts, *J. Am. Chem. Soc. 123*, 2970−2978.
30. Howarth, O. W., and Lilley, D. M. (1978) Carbon-13-NMR of peptides and proteins, *Prog. NMR Spectrosc. 12*, 1−40.
31. Wang, Y., and Jardetzky, O. (2002) Investigation of the neighboring residue effects on protein chemical shifts, *J. Am. Chem. Soc. 124*, 14075−14084.
32. Spera, S., and Bax, A. (1991) Empirical correlation between protein backbone conformation and Cα and Cβ nuclear magnetic resonance chemical shifts, *J. Am. Chem. Soc. 113*, 5490−5492.
33. Wishart, D. S., Sykes, B. D., and Richards, F. M. (1991) Relationship between nuclear magnetic resonance chemical shift and protein secondary structure, *J. Mol. Biol. 222*, 311−333.
34. Butner, K. A., and Kirschner, M. W. (1991) Tau protein binds to microtubules through a flexible array of distributed weak sites, *J. Cell Biol. 115*, 717−730.
35. Yao, J., Dyson, H. J., and Wright, P. E. (1997) Chemical shift dispersion and secondary structure prediction in unfolded and partly folded proteins, *FEBS Lett. 419*, 285−289.
36. Schwalbe, H., Fiebig, K. M., Buck, M., Jones, J. A., Grimshaw, S. B., Spencer, A., Glaser, S. J., Smith, L. J., and Dobson, C. M. (1997) Structural and dynamical properties of a denatured protein. Heteronuclear 3D NMR experiments and theoretical simulations of lysozyme in 8 M urea, *Biochemistry 36*, 8977−8991.
37. Bussell, R., Jr., and Eliezer, D. (2003) A structural and functional role for 11-mer repeats in α-synuclein and other exchangeable lipid binding proteins, *J. Mol. Biol. 329*, 763−778.
38. Chiti, F., Stefani, M., Taddei, N., Ramponi, G., and Dobson, C. M. (2003) Rationalization of the effects of mutations on peptide and protein aggregation rates, *Nature 424*, 805−808.
39. Konno, T., Oiki, S., Hasegawa, K., and Naiki, H. (2004) Anionic contribution for fibrous maturation of protofibrillar assemblies of the human tau repeat domain in a fluoroalcohol solution, *Biochemistry 43*, 13613−13620.
40. Hiraoka, S., Yao, T. M., Minoura, K., Tomoo, K., Sumida, M., Taniguchi, T., and Ishida, T. (2004) Conformational transition state is responsible for assembly of microtubule-binding domain of tau protein, *Biochem. Biophys. Res. Commun. 315*, 659−663.
41. Gamblin, T. C., King, M. E., Dawson, H., Vitek, M. P., Kuret, J., Berry, R. W., and Binder, L. I. (2000) *In vitro* polymerization of tau protein monitored by laser light scattering: Method and application to the study of FTDP-17 mutants, *Biochemistry 39*, 6136−6144.
42. Kelly, J. W. (1998) The alternative conformations of amyloidogenic proteins and their multi-step assembly pathways, *Curr. Opin. Struct. Biol. 8*, 101−106.
43. Morishima-Kawashima, M., and Ihara, Y. (2002) Alzheimer's disease: β-Amyloid protein and tau, *J. Neurosci. Res. 70*, 392−401.
44. Selkoe, D. J. (2001) Alzheimer's disease: Genes, proteins, and therapy, *Physiol. Rev. 81*, 741−766.
45. Serpell, L. C., and Smith, J. M. (2000) Direct visualisation of the β-sheet structure of synthetic Alzheimer's amyloid, *J. Mol. Biol. 299*, 225−231.
46. Petkova, A. T., Ishii, Y., Balbach, J. J., Antzutkin, O. N., Leapman, R. D., Delaglio, F., and Tycko, R. (2002) A structural model for Alzheimer's β-amyloid fibrils based on experimental constraints from solid-state NMR, *Proc. Natl. Acad. Sci. U.S.A. 99*, 16742−16747.

47. Tycko, R., and Ishii, Y. (2003) Constraints on supramolecular structure in amyloid fibrils from two-dimensional solid-state NMR spectroscopy with uniform isotopic labeling, *J. Am. Chem. Soc. 125*, 6606−6607.
48. Jaroniec, C. P., MacPhee, C. E., Bajaj, V. S., McMahon, M. T., Dobson, C. M., and Griffin, R. G. (2004) High-resolution molecular structure of a peptide in an amyloid fibril determined by magic angle spinning NMR spectroscopy, *Proc. Natl. Acad. Sci. U.S.A. 101*, 711−716.
49. Wishart, D. S., and Sykes, B. D. (1994) Chemical shifts as a tool for structure determination, *Methods Enzymol. 239*, 363−392.
50. Alexandrescu, A. T., Abeygunawardana, C., and Shortle, D. (1994) Structure and dynamics of a denatured 131-residue fragment of staphylococcal nuclease: A heteronuclear NMR study, *Biochemistry 33*, 1063−1072.
51. Eliezer, D., Yao, J., Dyson, H. J., and Wright, P. E. (1998) Structural and dynamic characterization of partially folded states of apomyoglobin and implications for protein folding, *Nat. Struct. Biol. 5*, 148−155.
52. Yao, J., Chung, J., Eliezer, D., Wright, P. E., and Dyson, H. J. (2001) NMR structural and dynamic characterization of the acid-unfolded state of apomyoglobin provides insights into the early events in protein folding, *Biochemistry 40*, 3561−3571.
53. Yi, Q., Scalley-Kim, M. L., Alm, E. J., and Baker, D. (2000) NMR characterization of residual structure in the denatured state of protein L. *J. Mol. Biol. 299*, 1341−1351.
54. Lacy, E. R., Filippov, I., Lewis, W. S., Otieno, S., Xiao, L., Weiss, S., Hengst, L., and Kriwacki, R. W. (2004) p27 binds cyclin−CDK complexes through a sequential mechanism involving binding-induced protein folding, *Nat. Struct. Mol. Biol. 11*, 358−364.
55. Radhakrishnan, I., Perez-Alvarado, G. C., Dyson, H. J., and Wright, P. E. (1998) Conformational preferences in the Ser133-phosphorylated and non-phosphorylated forms of the kinase inducible transactivation domain of CREB, *FEBS Lett. 430*, 317−322.
56. Zor, T., Mayr, B. M., Dyson, H. J., Montminy, M. R., and Wright, P. E. (2002) Roles of phosphorylation and helix propensity in the binding of the KIX domain of CREB-binding protein by constitutive (c-Myb) and inducible (CREB) activators, *J. Biol. Chem. 277*, 42241−42248.
57. Gustke, N., Trinczek, B., Biernat, J., Mandelkow, E. M., and Mandelkow, E. (1994) Domains of tau protein and interactions with microtubules, *Biochemistry 33*, 9511−9522.
58. Kar, S., Fan, J., Smith, M. J., Goedert, M., and Amos, L. A. (2003) Repeat motifs of tau bind to the insides of microtubules in the absence of taxol, *EMBO J. 22*, 70−77.
59. Minoura, K., Tomoo, K., Ishida, T., Hasegawa, H., Sasaki, M., and Taniguchi, T. (2002) Amphipathic helical behavior of the third repeat fragment in the tau microtubule-binding domain, studied by ^{1}H NMR spectroscopy, *Biochem. Biophys. Res. Commun. 294*, 210−214.
60. Minoura, K., Yao, T. M., Tomoo, K., Sumida, M., Sasaki, M., Taniguchi, T., and Ishida, T. (2004) Different associational and conformational behaviors between the second and third repeat fragments in the tau microtubule-binding domain, *Eur. J. Biochem. 271*, 545−552.
61. Lippens, G., Wieruszeski, J. M., Leroy, A., Smet, C., Sillen, A., Buee, L., and Landrieu, I. (2004) Proline-directed random-coil chemical shift values as a tool for the NMR assignment of the tau phosphorylation sites, *ChemBioChem 5*, 73−78.
62. Hamada, D., Segawa, S., and Goto, Y. (1996) Non-native α-helical intermediate in the refolding of β-lactoglobulin, a predominantly β-sheet protein, *Nat. Struct. Biol. 3*, 868−873.
63. Kuwajima, K., Yamaya, H., and Sugai, S. (1996) The burst-phase intermediate in the refolding of β-lactoglobulin studied by stopped-flow circular dichroism and absorption spectroscopy, *J. Mol. Biol. 264*, 806−822.
64. Balbach, J. J., Ishii, Y., Antzutkin, O. N., Leapman, R. D., Rizzo, N. W., Dyda, F., Reed, J., and Tycko, R. (2000) Amyloid fibril formation by A β 16−22, a seven-residue fragment of the Alzheimer's β-amyloid peptide, and structural characterization by solid-state NMR, *Biochemistry 39*, 13748−13759.
65. Balbirnie, M., Grothe, R., and Eisenberg, D. S. (2001) An amyloid-forming peptide from the yeast prion Sup35 reveals a dehydrated β-sheet structure for amyloid, *Proc. Natl. Acad. Sci. U.S.A. 98*, 2375−2380.
66. Lopez De La Paz, M., Goldie, K., Zurdo, J., Lacroix, E., Dobson, C. M., Hoenger, A., and Serrano, L. (2002) De novo designed peptide-based amyloid fibrils, *Proc. Natl. Acad. Sci. U.S.A. 99*, 16052−16057.
67. Booth, D. R., Sunde, M., Bellotti, V., Robinson, C. V., Hutchinson, W. L., Fraser, P. E., Hawkins, P. N., Dobson, C. M., Radford, S. E., Blake, C. C., and Pepys, M. B. (1997) Instability, unfolding, and aggregation of human lysozyme variants underlying amyloid fibrillogenesis, *Nature 385*, 787−793.
68. Jimenez, J. L., Guijarro, J. I., Orlova, E., Zurdo, J., Dobson, C. M., Sunde, M., Saibil, H. R. (1999) Cryo-electron microscopy structure of an SH3 amyloid fibril and model of the molecular packing, *EMBO J. 18*, 815−821.
69. Liu, Y., Gotte, G., Libonati, M., Eisenberg, D. (2001) A domain-swapped RNase A dimer with implications for amyloid formation, *Nat. Struct. Biol. 8*, 211−214.
70. Goedert, M., Jakes, R., and Crowther, R. A. (1999) Effects of frontotemporal dementia FTDP-17 mutations on heparin-induced assembly of tau filaments, *FEBS Lett. 450*, 306−311.
71. Rizzini, C., Goedert, M., Hodges, J. R., Smith, M. J., Jakes, R., Hills, R., Xuereb, J. H., Crowther, R. A., and Spillantini, M. G. (2000) Tau gene mutation K257T causes a tauopathy similar to Pick's disease, *J. Neuropathol. Exp. Neurol. 59*, 990−1001.
72. Barghorn, S., Zheng-Fischhofer, Q., Ackmann, M., Biernat, J., von Bergen, M., Mandelkow, E. M., and Mandelkow, E. (2000) Structure, microtubule interactions, and paired helical filament aggregation by tau mutants of frontotemporal dementias, *Biochemistry 39*, 11714−11721.
73. DeTure, M., Ko, L. W., Yen, S., Nacharaju, P., Easson, C., Lewis, J., van Slegtenhorst, M., Hutton, M., and Yen, S. H. (2000) Missense tau mutations identified in FTDP-17 have a small effect on tau−microtubule interactions, *Brain Res. 853*, 5−14.
74. Nacharaju, P., Lewis, J., Easson, C., Yen, S., Hackett, J., Hutton, M., and Yen, S. H. (1999) Accelerated filament formation from tau protein with specific FTDP-17 missense mutations, *FEBS Lett. 447*, 195−199.
75. Neumann, M., Schulz-Schaeffer, W., Crowther, R. A., Smith, M. J., Spillantini, M. G., Goedert, M., and Kretzschmar, H. A. (2001) Pick's disease associated with the novel Tau gene mutation K369I, *Ann. Neurol. 50*, 503−513.
76. Chou, P. Y., and Fasman, G. D. (1978) Empirical predictions of protein conformation, *Annu. Rev. Biochem. 47*, 251−276.
77. Lacroix, E., Viguera, A. R., and Serrano, L. (1998) Elucidating the folding problem of α-helices: Local motifs, long-range electrostatics, ionic-strength dependence, and prediction of NMR parameters, *J. Mol. Biol. 284*, 173−191.
78. Schweers, O., Mandelkow, E. M., Biernat, J., and Mandelkow, E. (1995) Oxidation of cysteine-322 in the repeat domain of microtubule-associated protein tau controls the *in vitro* assembly of paired helical filaments, *Proc. Natl. Acad. Sci. U.S.A. 92*, 8463−8467.
79. Gamblin, T. C., King, M. E., Kuret, J., Berry, R. W., and Binder, L. I. (2000) Oxidative regulation of fatty acid-induced tau polymerization, *Biochemistry 39*, 14203−14210.
80. Barghorn, S., and Mandelkow, E. (2002) Toward a unified scheme for the aggregation of tau into Alzheimer paired helical filaments, *Biochemistry 41*, 14885−14896.
81. Terry, C. J., Damas, A. M., Oliveira, P., Saraiva, M. J., Alves, I. L., Costa, P. P., Matias, P. M., Sakaki, Y., and Blake, C. C. (1993) Structure of Met30 variant of transthyretin and its amyloidogenic implications, *EMBO J. 12*, 735−741.
82. McCutchen, S. L., and Kelly, J. W. (1993) Intermolecular disulfide linkages are not required for transthyretin amyloid fibril formation *in vitro*, *Biochem. Biophys. Res. Commun. 197*, 415−421.

BI048953N